LAWRENCE
LIVERMORE
NATIONAL
LABORATORY

UCRL-JRNL-227339

Growth and stability of oxidation resistant Si nanocrystals formed by decomposition of alkyl silanes

N. Zaitseva, S. Hamel, Z. R. Dai, C. Saw, A. J. Williamson, G. Galli

January 19, 2007

Journal of Physical Chemistry - C

Updated October 14, 2003

Growth and stability of oxidation resistant Si nanocrystals formed by decomposition of alkyl silanes

N. Zaitseva, S. Hamel, Z. R. Dai, C. Saw, A. J. Williamson, G. Galli

Abstract. The synthesis and characterization of 1-10 nm Si nanocrystals highly resistant to oxidation is described. The nanocrystals were prepared by thermal decomposition of tetramethylsilane at 680^{o}C, or in a gold-induced catalytic process at lower temperatures down to 400-450^{o}C using trioctylamine as an initial solvent. Transmission electron microscopic analysis of samples obtained in the presence of gold show that the nanocrystals form via solid-phase epitaxial attachment of Si to the gold crystal lattice. The results of computational modeling performed using first principles density functional theory (DFT) calculations predict that the enhanced stability of nanocrystals to oxidation is due to the presence of N or N-containing groups on the surface of nanocrystals.

I. Introduction

The possibility of using Si-based light-emitting devices for optoelectronic applications[1] has stimulated intensive studies aimed at the development of new methods of producing nanosized Si particles and characterization of their structure and optical properties. Dispersions of uniform size colloidal nanocrystals (NCs) produced by solution techniques have shown the most promise for synthesizing Si NCs with relatively monodisperse size distributions needed for comprehensive studies of their properties. Some of these techniques developed in recent decades include gas-phase decomposition of silanes,[2-4] ultrasonic dispersion of porous silicon, [5-7] etching of bulk Si,[8,9] direct chemical synthesis,[10,11] inverse micelles, [12] laser driven pyrolysis,[13] aggregation of atoms in a vacuum,[14] and high temperature-pressure experiments.[15-17] Despite the obvious progress achieved in these studies, the challenge still remains to create well-defined

particles with the tightly controlled size and size distribution needed for experimental and theoretical studies of photoluminescence (PL). The origin of this PL is the subject of continuing debates that involve two competing mechanisms - quantum confinement effects in the crystalline cores and luminescence from the surface states which can substantially depend on the synthetic methods. Large discrepancies in the PL peak energy attributed to the same size of NCs produced by different techniques[12] can be also affected by oxidation process[18,19] and by the contribution from luminescent by-products of the reactions. A full understanding and separation of these effects requires more attention to the characterization methods and crystallization mechanisms, which can be used for further development of reproducible techniques to obtain large amounts of isolated, stable Si NCs with narrow size distribution and well-controlled surface passivation.

In this paper, we describe one of such mechanisms observed with colloidal Si NCs obtained by decomposition of organosilane precursors. We show that the high temperature typically needed for the formation of highly crystalline Si NCs can be reduced by the Au-induced crystallization that proceeds, however, not through the traditional Vapor-Liquid-Solid (VLS) mechanism but via epitaxial growth of Si NCs on the Au crystal lattice. Additional consideration is given to stability of the NCs to oxidation analyzed on the basis of the experimental results combined with first principles density functional theory (DFT) calculations.

II. Experimental section.

High-temperature metal reactor syntheses were carried out in a 22 ml metal (Hastelloy) vessel. This method can be considered as a version of pressure-temperature experiments

used previously[16, 17] with the difference that, since practically all organic solvents decompose at the temperatures of experiments (550-700^{o}C), we did not operate in terms of supercritical conditions paying more attention to the temperature that produced major effect on the precursor decomposition and crystallization process. Tetramethylsilane (TMS, Gelest, 99.9%) and tetraethylsilane (TES, Gelest, 99%) were used as precursors in a typical amounts of 5 ml (3.205 g and 3.83 g, respectively) in the absence of additional solvents. Initially, these precursors were chosen for two major reasons: (1) to reduce the amounts of decomposition products, due to the minimum length of the organic chains in their structure, and (2) to avoid formation of luminescent by-products that may screen the PL produced by NCs, as it typically happens when aromatic rings are present (for example, pure toluene heated in the Hastelloy reactor to 680^{o}C decomposes to substances that produce bright-orange PL). In the reactions with amines, the precursor was made as a mixture of TMS or TES with trioctylamine (TOA, $[CH_3(CH_2)_7]_3N$) in the Mol ratio of about 1:1. When gold was used as a catalyst, a few drops of commercially produced gold nanoparticle solutions (Ted Pella, 2 nm) were vacuum-dried in the reactor prior to the introduction of the precursor. The precursor was introduced into the reactor in an Ar glovebox, sealed hermetically, and placed into a gradually heated furnace. After the furnace was heated to a desired level, the reaction was carried out at a constant temperature during about one hour. Reactions were terminated by a simple removal of the reactor from the furnace and cooling to room temperature. The reactor was open in air, the final product was washed several times by ethanol combined with centrifuging and dried under nitrogen. The dry powder did not dissolve in any of regular solvents, like toluene, hexane or chloroform, but was easily dispersed and partially dissolved in *N*,*N*-

dimethylformamide (DMF, $HCON(CH_3)_2$) which was used as a solvent for sample preparation.

Glassware syntheses were made in a standard 250 ml three-neck heavy-wall Pyrex flask connected to a vacuum/inert gas (Schlenk) line. The same precursors of pure TMS, TES or their mixtures with TOA were prepared in a glovebox. For the catalytic reactions, dry 5 nm-gold particles were added in a small amount which produced no visible coloration of the precursors. The reaction flask was evacuated at 110°C to a level below 100 mtorr, and then disconnected from the vacuum line. Since the glass reactor connections were not designed to withstand the more than 1 atm pressures created during the heating process, only 1-2 ml of a precursor were injected into the flask. The flask was heated by a high-temperature mantle (Chemglass) that enabled the reagents to reach temperatures up to 650°C. The reaction was terminated by the removal of heat immediately after a thin layer of a dark solid (typically at 400-450°C) formed from the colorless vapor, and the flask was opened to argon to remove the gaseous products of the reaction. When TOA was used, the Ar connection was opened after the condensation of the residual amine became visible on the glass walls (the boiling point of TOA is about 382°C). After cooling to room temperature, toluene was added to the flask. The final product was separated from the glass by stirring or sonication, centrifuged, dried under nitrogen and dispersed in DMF for further analysis. Transmission electron microscopy (TEM) images were obtained at UC Berkeley using a Tecnai-12 TEM with accelerating voltages of 100kV. High resolution TEM (HRTEM) and elemental analysis were made at Lawrence Livermore Laboratory with a Philips CM300FEG and High Angle Annular Detector Dark Field Scanning TEM

microscope (HAADF STEM) with accelerating voltage of 300 kV and 200 kV respectively. X-ray diffraction (XRD) was acquired using a CPS 120 INEL curved position sensitive detector system utilizing Cu Kα radiation.

III. Simulation Methods

We performed a series of first principles density functional theory (DFT) calculations of 1nm silicon clusters, terminated with hydrogen and various carbon or nitrogen containing groups. The calculations were made within the Perdew-Burke-Ernzerhof[20] (PBE) generalized gradient approximation to the exchange-correlation functional. For each cluster, the atomic coordinates were relaxed to the closest local minimum of the potential energy surface and then the electronic properties were calculated for the relaxed structure. The calculations use norm conserving, Troullier-Martins pseudopotentials and a plane-wave basis with a 70 Ry cutoff for the clusters involving carbon and nitrogen. The simulation supercell sizes were chosen to place more than 10 Å of vacuum between the periodic replica of the Si NCs, so as to remove any interactions. The atomic relaxations were performed until the residual force on all atoms was lower than $3 \cdot 10^{-3}$ eV/Å. The QBOX[21] code was used for the structural relaxations.

IV. Experimental results and discussion

Metal reactor synthesis. According to the previous reports[22-24] the decomposition of TMS and TES goes with the formation of elemental Si and gas products that essentially form upon pyrolysis of ethane (C_2H_4, CH_4, H_2 and C). In our experiments made in the absence of added catalysts, the final solid contained mainly amorphous product with a large

concentration of Si, detected by Energy Dispersive Spectroscopy (EDS). When TES was used as a precursor, no crystalline Si was detected in the final amorphous powder even if the syntheses were carried out at 700^{o}C. Formation of NCs was observed only in the syntheses with decomposition of TMS at temperatures as high as 680^{o}C

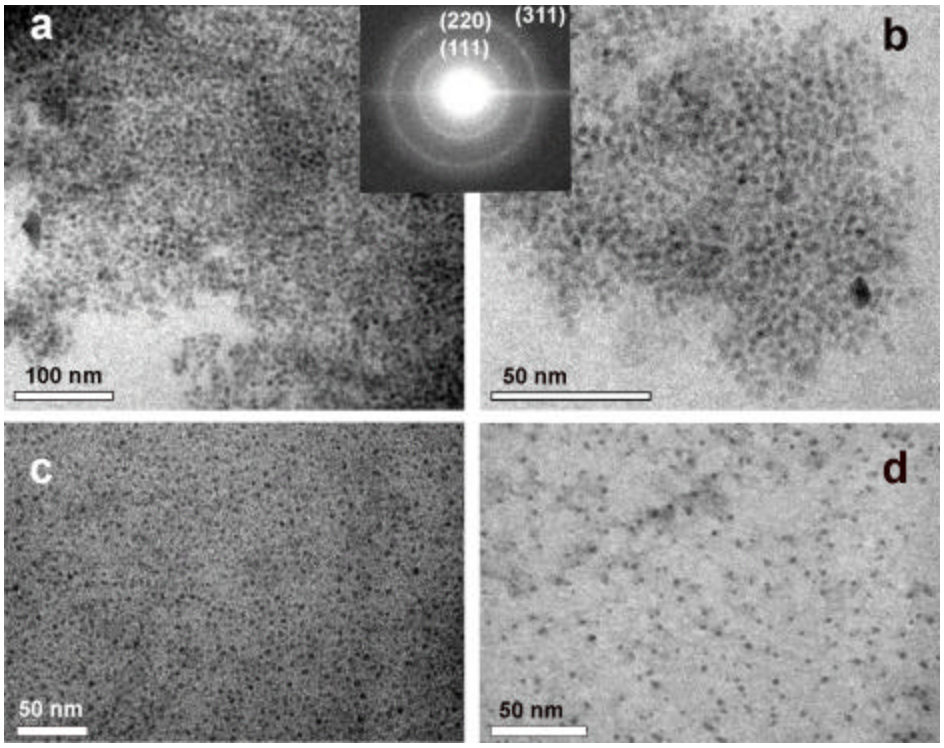

Fig.1. TEM images of Si nanocrystals synthesized in a metal reactor: (a) and (b) – 680^{o}C, TMS with TOA, no catalyst; (c) and (d) – 600^{o}C, TES with TOA and 2 nm gold particles; an electron diffraction pattern (insert) corresponds to d-spacing: 3.13 Å (111), 1.93 Å (220), 1.63 Å (311) of cubic diamond structure of Si.

(Figure 1, a and b). Electron diffraction patterns (insert to Figure 1) obtained from extended selected areas containing NCs undeniably corresponded to pure diamond Si. The typical size of the nanocrystals was about 5 nm (Figure 2 a) with the size distribution within a factor of two. It should be noted that the size of NCs never exceeded 10 nm, and formation of polycrystalline or macroscopic-scale Si crystals was not observed in any of the syntheses. HRTEM analyses made with the NCs revealed highly crystalline

structures with clearly seen planes and individual columns of atoms even in the smallest NCs with sizes close to 1 nm that should contain only about 35 Si atoms (Figure 2 b). Spherical 2nm and 5nm Si NCs have respectively 191 and 3133 Si atoms.

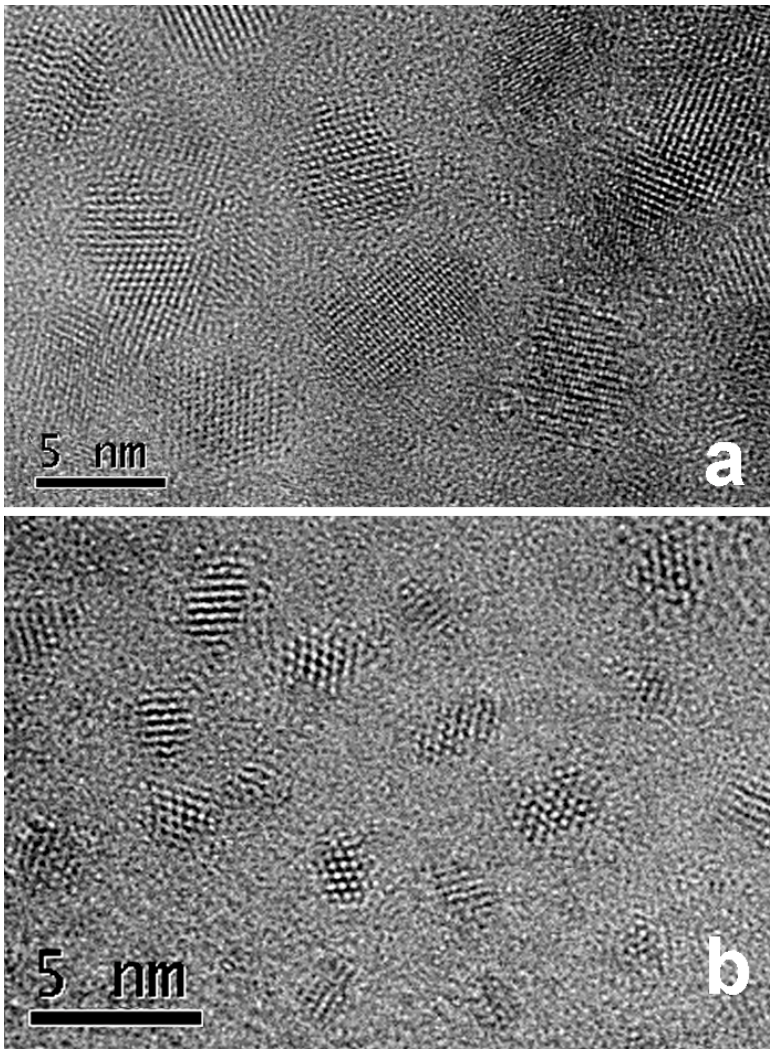

Figure 2. HRTEM images of nanocrystals synthesized in a metal reactor in the presence of TOA; measured distances between the planes correspond to (111) and (220) d-spacing of cubic diamond Si.

Despite the remarkable quality of the individual NCs presented in Figures 1 and 2, it should be, however, admitted that high temperatures of the syntheses produced noticeable difficulties for controlling the reaction conditions. The very narrow temperature range

limited from below by the lack of crystallization, and from above by technical difficulties, did not allow for establishing any effect of the temperature on the size and properties of NCs. Additional difficulties were introduced by the large impact of organic pyrolysis[25] and possible reactions with the material of the reactor for temperatures above 600°C (temperature of the commercial specification of the Hastelloy reactor). In the attempts to decrease the crystallization temperature, 2 nm Au nanoparticles were used with the initial goal that catalytic decomposition of the precursors will result in the formation of the Si nanowires according to the VLS mechanism.[26,27] With the use of the gold nanoparticles, crystalline Si could be detected in the final product of the reactions conducted with both TMS and TES in the lower temperature region of 450-600°C. However, unexpectedly, almost no nanowires were observed, and NCs had rather isometric shape (Figure 1, c and d) close to that obtained in non-catalytic syntheses. Another surprising result was that in many cases, Si NCs were found apart from Au nanoparticles in the amounts larger than that expected if only one Si NC would catalytically form on a corresponding Au nanoparticle.

Glassware synthesis. A partial explanation to the phenomena of isometric Si NCs formation on the Au nanoparticles was found from the results of the experiments made in glassware. A known advantage of this method is that the reaction can be directly observed and therefore monitored in time. In addition, the fact that the vessel can be easily connected to the vacuum of inert gas line allows for a simple removal of the gaseous products at any moment of the reaction. The amount of solid obtained in such reactions was extremely small but still enough for TEM analysis which indicated higher

fraction of crystalline Si in comparison with the metal reactor synthesis. Bigger Au nanoparticles (with an average size of 5 nm) were used to obtain better TEM resolution.

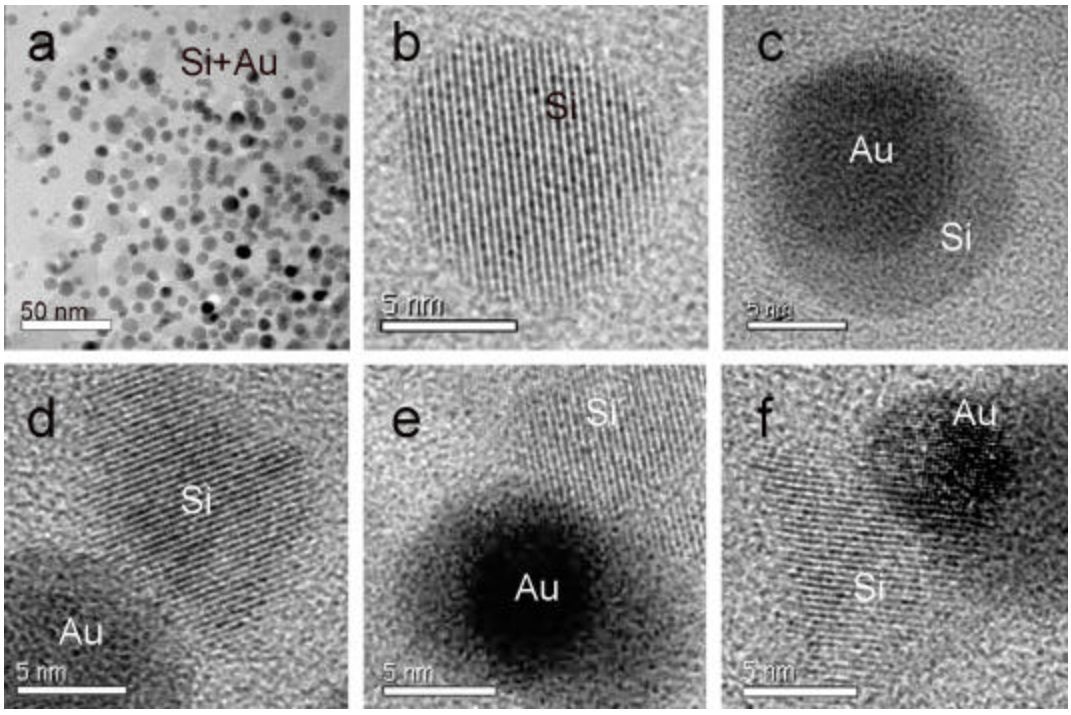

Figure 3. Si nanocrystals formed in a glass flask at 450°C in the presence of gold nanoparticles and: (a) – low resolution image of mixture of Si (low contrast) and Au (high contrast) nanoparticles ; (b) – HRTEM image of a free-standing Si nanocrystal; (c) – HRTEM image of a gold nanoparticle with an amorphous Si shell; (d–f) HRTEM images of Si nanocrystals attached to gold nanoparticles.

Typical images of NCs obtained with the final products of the glassware reactions show groups of nanoparticles with clearly pronounced different TEM contrast (Figure 3a). HRTEM analysis of these particles, combined with EDS, shows that they consist of (1) initial Au NCs (dark contrast in Figure 3a) , (2) free-standing Si NCs with the light contrast (Figure 3, a and b), (3) Au particles with amorphous Si shells (Figure 3c), and Au nanoparticles with Si NCs attached to them (Figure 3, d-f). Test experiments made under the same conditions in the absence of Au nanoparticles showed no sign of the decomposition of both precursors, indicating that gold does serve as a catalyst in the precursor decomposition and Si formation process. A simplest explanation of this process

would be the VLS mechanism which takes place when atomic Si produced in the catalytic decomposition first dissolves in a gold nanoparticle, and then is expelled from it as a thin crystalline nanowire[27]. Although the classical VLS mechanism[26] requires presence of liquid gold, it has been shown that it also may proceed at temperatures much below Au melting point due to the formation of thin liquid eutectic layers on the surface of solid gold nanoparticles.[28,29] There is, however, a contradiction that makes it difficult to refer to the VLS mechanism in the case of the NCs shown in Figure 3. When the

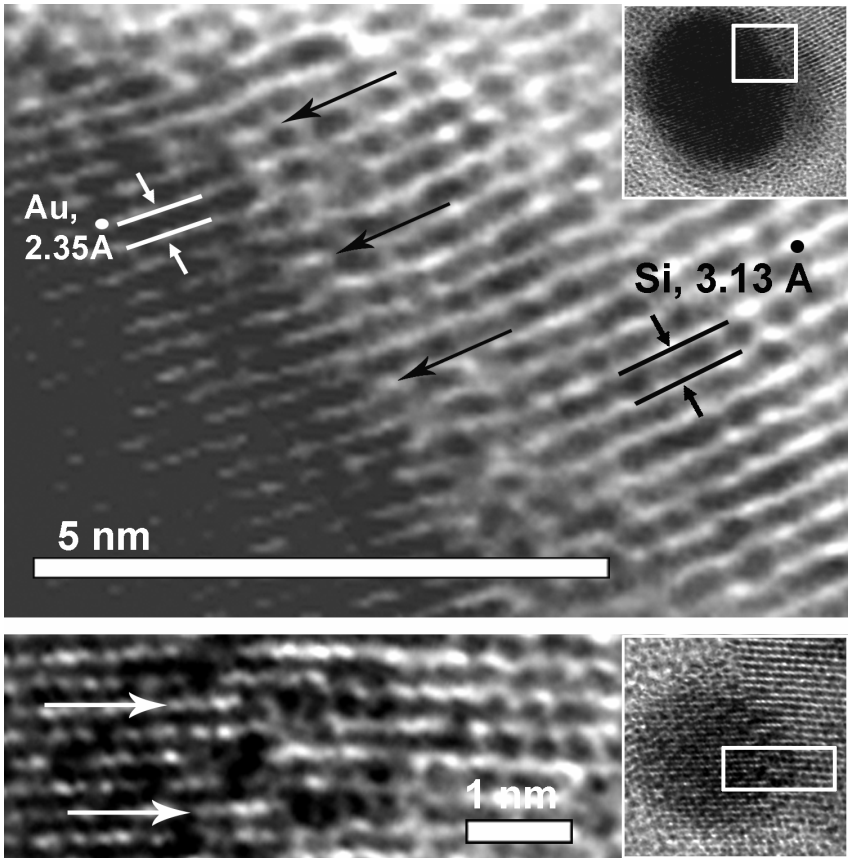

Fig. 4. HRTEM images of the interface boundaries between Au and Si crystallographic lattices. Corresponding areas are squared in lower magnification images of joint Au/Si NCs (inserts). Crystalline Si epitaxially formed on the gold nanoparticles. The difference between {111} d-spacings is compensated by formation of misfit dislocations (shown by arrows as extra planes in the gold lattice).

growth of Si takes place according to the VLS mechanism, the deposition of Si atoms occurs from the liquid interface between Au and Si, leading to the fact that Si crystal lattice forms independently of the crystallographic structure of the catalyst. The situation is rather different with the particles obtained in our experiments. HRTEM images of joint Au-Si NCs show that in many cases (111) planes of Si directly continue same simple indexes planes of gold (Figure 3f and Figure 4). Such connection between two crystallographic lattices is possible only if during crystallization process initial Si atoms epitaxially attach directly to the Au crystal lattice, and further growth of Si NCs proceeds not by deposition from the liquid interface between Au and Si, but rather by the attachment of atoms to the Si layers on the side opposite to the gold nanoparticle. Si atoms needed for such attachment may come from the amorphous layer around gold nanoparticles, similarly to the process of metal-induced crystallization of thin amorphous Si layers.[30] It is known that in the absence of metal catalysts, crystallization of Si from the amorphous phase takes place in the temperature range of 600-700^{o}C relying on the crystalline Si substrate to promote epitaxial crystallization.[31] When small metal particles (Au, Ni) are present, the range of Si crystallization shifts to lower temperatures of 250-600^{o}C.[32] Metal-induced crystallization of amorphous Si is attributed to an interaction of the free electrons of the metal with neighboring Si atoms by reducing the strength of the covalent Si bonds near the growing interface.[32] Although crystallization of amorphous Si in the presence of gold is a known phenomenon, it proceeds through the formation of Au/Si alloys,[30] and no epitaxial growth has been reported for this process. Solid-phase epitaxial growth of Si was observed[31] from the layer of $NiSi_2$ which has very close (111)-spacings (3.12 Å) to that of Si (3.13 Å). The results of our experiments present the

evidence that similar epitaxial growth of Si can occur on gold nanoparticles. However, HRTEM images do not reflect any intermediate Au/Si alloys. Figure 4a shows that the structure of the boundary between two single crystals periodically contains three (111) Si planes formed on corresponding Au planes. Each forth Si plane (shown by black arrows) is formed on a pair of gold planes. The extra planes in the gold crystal lattice, more clearly seen in Figure 4b (white arrows), represent classical examples of misfit dislocations formed to compensate the difference in the interplanar distances between two adjacent crystal lattices. Extremely large difference (33%) in the d-spacings of joint (111) planes of Si and gold (2.35 Å for Au and 3.13 Å for Si) should lead to a big stress on the interface resulting in formation of a very small width of the epitaxial bridge and its eventual destruction, as it is seen in the lower right area of Figure 4a. These conditions may result in easy separation of NCs making it possible for Au nanoparticles to serve as catalysts multiple times. Although it is only a speculation, this separation can explain the formation of the free-standing Si NCs found in large numbers without Au nanoparticles. Small size of the NCs may also relate to the gold catalytic effect. Since the decomposition of precursors is catalyzed by Au nanoparticles, amorphous Si needed for crystallization is available only in a close vicinity to the surface of gold. This condition makes the size of the final Si NCs comparable to the size of gold nanoparticles.

The availability of the amorphous Si produced as a result of TMS and TES decomposition most likely determines the mechanism of Si NCs formation in the presence of Au. At the same time similar effect from other metals cannot be also completely excluded even if the NCs were formed without added catalysts but in a metal reactor (like Si NCs shown in Figure 1, a and b). EDS and electron energy loss

spectroscopy (EELS) analyses made with the final products of our experiments frequently showed the presence of Ni or Fe (main constituents of the Hastelloy) known as efficient initiators of the metal-induced crystallization of Si.[31] Some randomly formed structures directly containing these metals or known to be formed in their presence

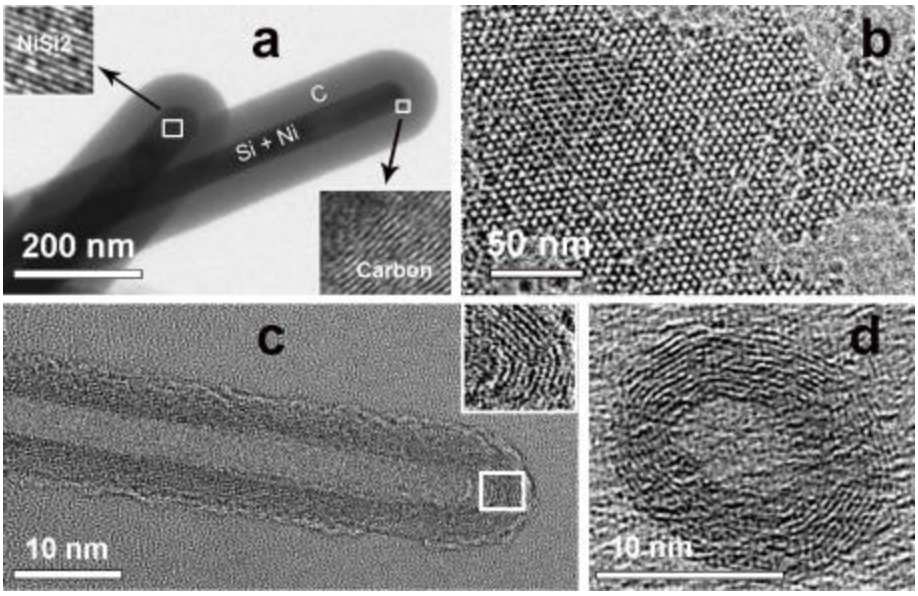

Fig.5. Side products of Si NC metal reactor syntheses: (a) - rods containing Si and Ni in a carbon (graphite) shell; (b) – assembly of FeSi nanocrystals; (c) - carbon nanotube; (d) – carbon nano-onion. The composition was detected by EDS and EELS analyses. The inserts show HRTEM images corresponding to squared areas.

(Figure 5) show that the interaction of Si precursors with these metals should be taken into consideration when the reactions are carried out in metal reactors. In the case when other mechanisms are studied, a practical solution to avoid such interaction would be the use of glass or quartz liners inside the metal reactors.

Stability of NCs. Stability of NCs to oxidation is one of the most important properties that provide conditions for more complete characterization and potential applications. All Si NCs obtained in our experiments remained stable for a few weeks after the reactors were opened in air. This fact indicates that the surface of the NCs was protected from fast

oxidation by some passivation layer. In the case when no solvents were added to the initial precursor mixtures, the most likely candidates for the surface passivation would be the alkyl groups or hydrogen forming in the reactions of TMS or TES decomposition.[22-24] Our observations showed that despite of the initial stability to oxidation, when analyses of such samples, synthesized with pure TMS or TES, were repeated after 2-3 months, Si NCs were found in much smaller amounts with visibly degraded crystallinity. The situation was noticeably different in the cases when trioctylamine (TOA), or in some case lower amines, were used as solvents in the initial precursor mixtures. HRTEM images of Figure 2, for example, were taken from the TEM grids exposed to air during five months after they first were detected by low resolution TEM. These images show that even very

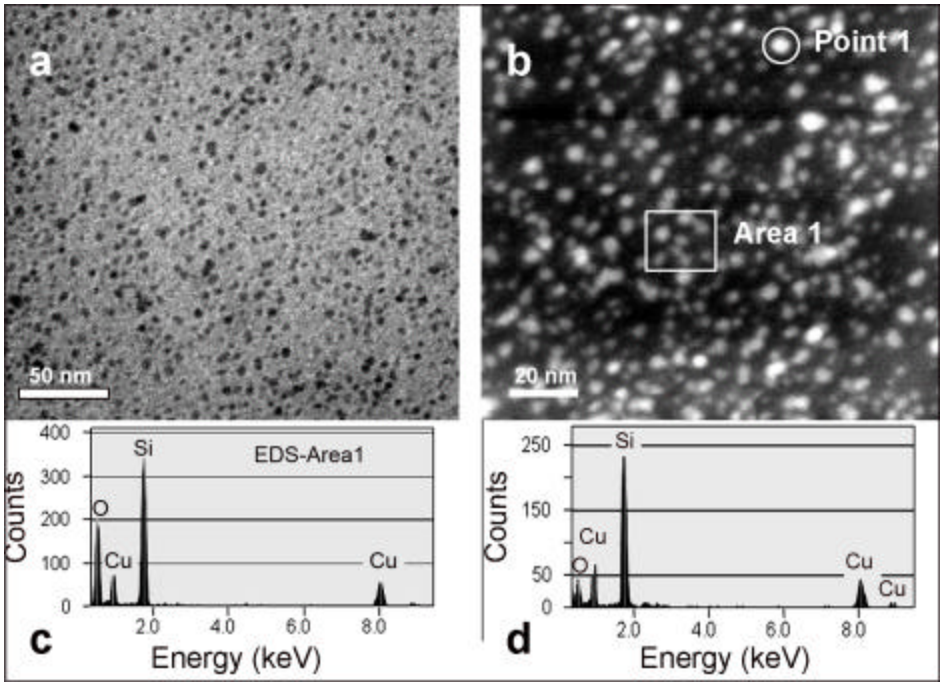

Fig. 6: TEM (a) and HAADF STEM (b) images of Si nanocrystals obtained from a DMF solution of a dry powder exposed to air during one year; (c) and (d) - EDS patterns showing Si with only traces of oxygen in individual nanocrystals (point 1 in image b) compared to higher average concentration of the residual oxygen on the TEM grid (area 1). Copper signal is scattered from the grid.

small NCs with sizes close to 1 nm preserved their perfect structure without oxidation. More analyses which included HAADF STEM imaging (Figure 6) showed that Si NCs synthesized in the presence of amines could freely resist oxidation during time periods over a year. Unfortunately, since K-edge of the nitrogen X-ray absorption is in the absorption range of the EDS detector, it is not easy to directly detect small concentrations of nitrogen on the surface of nanocrystals using TEM analyses. Application of other techniques, like Fourier Transform Infrared (FTIR) analysis, Raman spectroscopy, or Secondary Ion Mass Spectroscopy (SIMS) requires more work on achieving a complete separation of NCs from the amorphous by-products, also containing Si and N. Computational modeling allows us to bridge this gap by predicting in detail the influence of the atomistic surface structure on the properties of Si NCs in the absence of complete experimental data. Blank experiments made with TOA showed that ammonia is always one of the products of its decomposition at the temperatures above 600^{o}C. This fact presents experimental evidence that at these temperatures amines go through the transformations resulting in the break of C-N bonds with formation of lower amines, nitrogen or ammonia which can readily attach to the Si surface.[33] Based upon our simulations of the interaction between Si nanoclusters and N- and C-containing functional groups (see section V), we conjecture that the enhanced stability of S-nc's to oxidation may be connected with the presence of nitrogen containing groups on the surface of the nanocrystals.

Photoluminescence. Final products obtained with all syntheses described above produced visible PL upon the excitation by UV light (Figure 7a). Since blank experiments made with TOA and some linear chain alkanes (pentane, hexane) under the same conditions did

not result in luminescent products, this PL should be undeniably related to the presence of Si or silicon containing compounds. There are, however, certain concerns which do not allow us to attribute the spectra presented in Figure 7a only to Si NCs. The main problem relates to the low yield of Si NCs and experimental difficulties of their separation. Despite the fact that areas filled with NCs similar to those shown in Figures 1 and 2 were detected in TEM analysis, macroscopic X-ray diffraction (XRD) of the final powders produced in metal reactors typically showed pure amorphous structures. XRD patterns with weak Si peaks (Figure 10b) were obtained only during long counting times (over several days) using small amounts of material collected in the process of multiple cleaning procedures. However, even in these cases XRD patterns always showed the presence of a large amorphous fraction which according to EDS analysis contained Si as its main constituent. Inclusions of C and sometimes other unidentified compounds that could vary from one sample to another could also be observed in some samples (upper XRD spectrum of the Figure 7b). It should be noted that when 2 nm gold nanoparticles were used, Au peaks never appeared in the final XRD patterns indicating that the weak reflection from such small particles can be easily screened by the stronger amorphous signal. It also can be considered as one more confirmation that Si NCs formed in the amounts exceeding the amounts of the initially used gold catalyst. The fact that PL could be freely observed in the macroscopic measurements independently of the presence or absence of crystalline phase indicated that the amorphous fraction should introduce major contribution into the total luminescence. In addition, the absence of any correlation with the size of Si NCs could also indicate that the variations in the peak energy position of the PL spectra was determined not by quantum confinement effect, but more likely by the

composition and structure of this amorphous fraction. There is, however, one qualitative correlation found in analysis of all PL spectra. As shown in Figure 7a, the spectra of all samples produced in the metal reactor syntheses with TOA were located in the orange-red range of the optical region. Blue-green PL was more common for the samples synthesized without amines and for all syntheses conducted in glassware where decomposition of amines did not occur due to the lower temperature range. If the PL presented in Figure 7a were produced by Si NCs, the difference in the peak position of

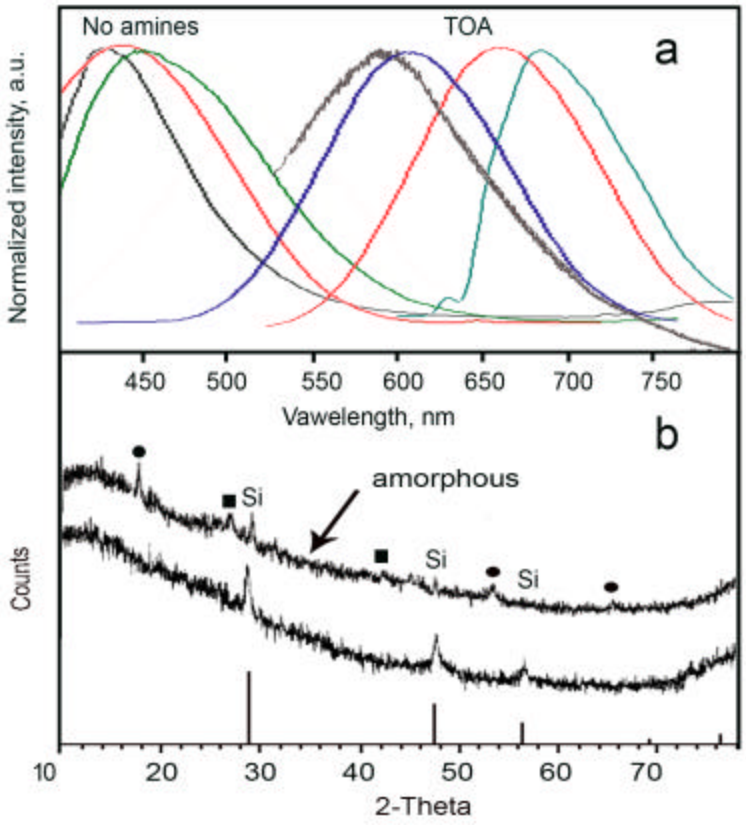

Fig. 7. a – typical photoluminescence spectra of the final powders dispersed in DMF; exc itation wavelength is 400 nm; b – XRD patterns of a final solids obtained in multiple cleaning procedures; ¦ – possible carbon (graphite), ? – unidentified crystalline products; vertical bars on horizontal axis show the standard XRD pattern of the diamond Si in Cu Kα radiation.

two groups of spectra could be explained by the difference in the surface termination. As already mentioned above, the decomposition of pure TMS and TES goes through the

formation of hydrogen[22-24] that is one the most likely candidates for the surface passivation in the experiments conducted in the absence of amines. According to calculations[34], replacement of hydrogen by N or N-containing groups should decrease the band gap energy of Si nanoclusters leading to the shift of PL spectra to the region of longer wavelength. However, the low yield of Si NCs and the domination of the amorphous fraction in the optical properties of the samples does not allow us to establish such direct correlations without understanding the nature of the PL produced by the amorphous fraction and its relevance to the structure and composition of Si clusters. Small amorphous Si clusters (1 to 5 nm) are known to show luminescence[34-37] and could be responsible for the broad spectra that were obtained were they to be present in large number in the amorphous by-product. The resolution of these problems will be addressed on the next stages of this work.

V. Computational modeling of silicon nanocrystals.

The remarkable stability against oxidation of the observed Si NCs structures points to the presence of a passivating layer on the surface of the clusters. On the basis of our DFT electronic structure simulations, we show that when present, N is more likely to be on the surface than in the core of a Si NC. We also show that if the conditions are right to have one N on the surface, then multiple N coverage is also likely. We propose that nitrogen plays a key role in that passivating layer.

To identify the relevant Si NCs structures to study, we first address the solubility of nitrogen in crystalline silicon at the nanoscale. Nitrogen is known to have a very low solubility in bulk Si.[38] Previous calculations[39,40] have shown that a single N interstitial

shows a fast diffusion through the crystal until it is trapped by other defects such as a second N interstitial. This di-interstitial nitrogen pair was identified as the most common defect in bulk silicon.[41] In the context of NCs, the high mobility of a single N interstitial would quickly move it to (or keep it on) the surface of a growing Si NC. One can envision a pair of N interstitials getting trapped in the core of the cluster (Figure 8a) but our calculations show that a similar configuration at the surface (Figure 8b) is energetically favored by 0.7 eV. This is due to a minimization

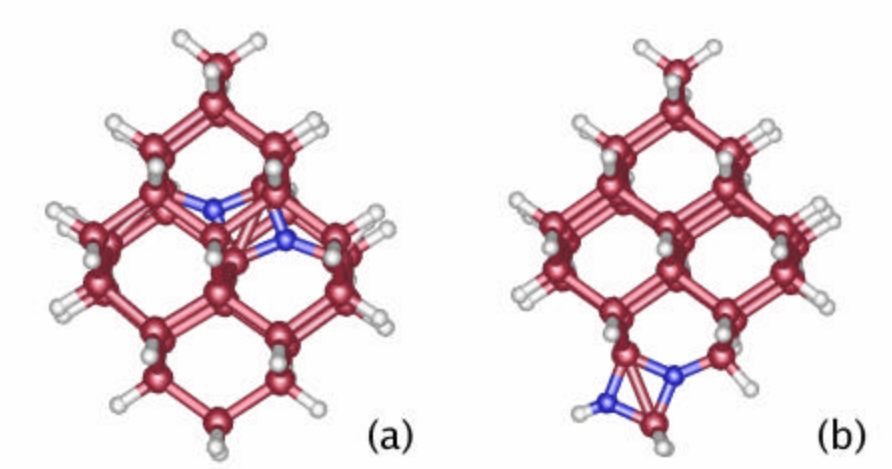

Figure 8. A comparison of the structures of Si nanocrystals containing a di-interstitial nitrogen defect (a) in the core, and (b) on the surface.

of the stress on the crystalline core when the di-interstitial pair of N is at the surface.

Structure and relative stability of N dopants. Considering the low solubility of defects in Si NCs, we concentrate our study on surface N groups. A representative set of the N-doped Si NCs calculated in this work are shown in Figures 8, 9 and 10. Our reference H-terminated 1nm Si NC consists of a diamond crystalline core of 35 Si atoms where dangling bonds are capped with 36 H atoms. For all the nitrogen doped clusters, in keeping with known molecules containing N, Si and H atoms such as disilazane, trisilylamine or studies of the dissociative adsorption of ammonia on silicon surfaces,[42,43]

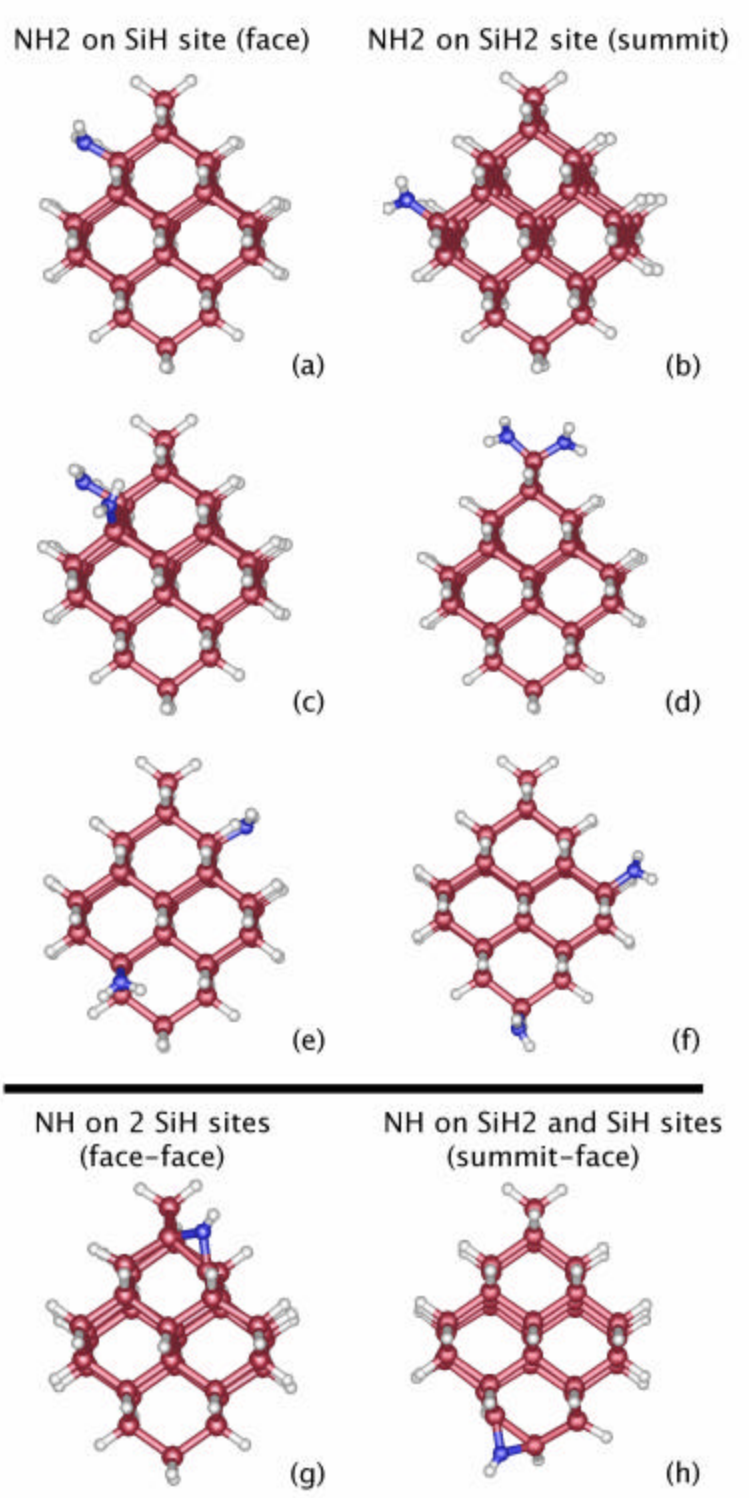

Figure 9. Silicon atoms are red, nitrogen atoms are blue and hydrogen atoms are light grey. Structures (a), (c) and (e): the amine groups are replacing H atoms from SiH sites (face of the Si NCs). Structures (b), (d) and (f): the amine groups are replacing H atoms from SiH_2 sites (summit of the Si NCs). In structure (g) and (h), a NH group is replacing two H atoms from SiH sites (face-face) and one H atom from a SiH_2 site and one from a SiH site (summit-face).

nitrogen is three-fold coordinated. In structures 9(a) through 9(f), a surface hydrogen is replaced with an amine group.

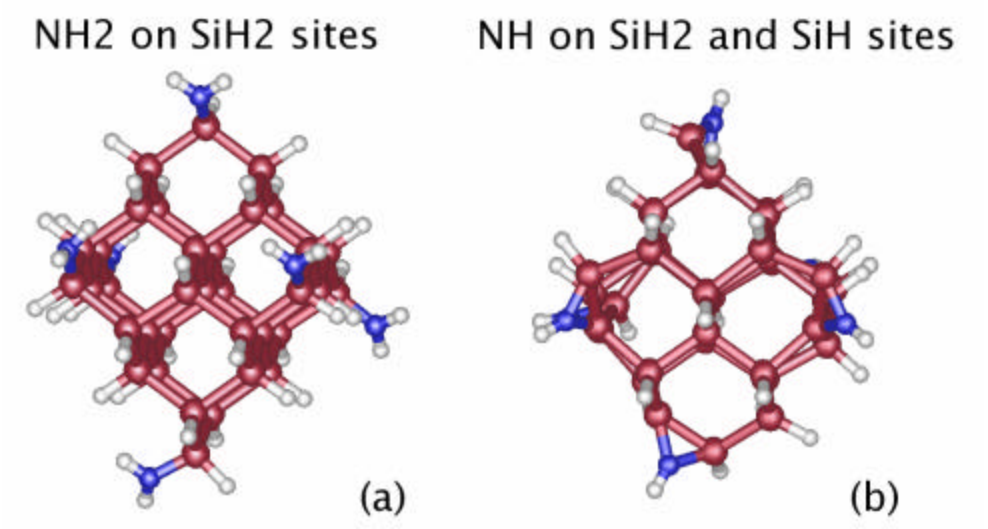

Figure 10. Silicon atoms are red, nitrogen atoms are blue and hydrogen atoms are light grey. Structures (a) has 6 amine groups on SiH_2 sites. Structure (b) has 6 NH groups bonded to a SiH_2 site and s SiH site.

We focus on two types of surface N groups: a NH_2 substituting a H atom and a bridged NH substituting two H atoms, and consider the effect of multiple N groups on the surface of Si NCs. In the case of oxygen dopants, Puzder et al. have shown[18] that the energy differences associated with the addition of a second oxygen group were within 0.1 eV of that for adding the first oxygen and that this remained true until the cluster was completely covered both with either double bonded or bridged oxygen. Therefore, from a purely thermodynamic perspective, if the chemical potentials of hydrogen and oxygen are such that it is favorable to replace surface hydrogen atoms with oxygen atoms, the oxygenation reaction is likely to continue until the nanocluster is completely covered with oxygen. We follow the same approach in the case of N groups. We first calculated the difference in the total energy of the reference clusters $Si_{35}H_{36}$ and $Si_{35}H_{35}NH_2$ where

the amine group is replacing a hydrogen of the original cluster (Figure 9: structures (a) and (b)). We then calculated the difference in total energy between a cluster with one and two amine groups with the amine groups either alongside or on opposite sides of the cluster (Figure 9: structures (c), (d), (e) and (f)). This provides an estimate of the steric repulsion between the amine groups which is lower than 0.1 eV. This is comparable to the energy difference associated with the addition of a second amine group and this remained true up to six amine groups. This means that it is just as favorable to add the sixth amine group as it is the first. Calculations with the bridged N configuration showed similar results. Therefore, we also predict that if the conditions are such that it is favorable to replace surface hydrogen atoms with a nitrogen containing group, multiple coverage with nitrogen groups is likely to occur. This conclusion holds for small nitrogen groups (NH,NH_2). For larger surface groups, steric interactions between the groups may play a more important role.

Relative Stability of N and C surface dopants. The precursor molecules (TMS, TES) used during the colloidal growth of Si NCs contain numerous carbon atoms. Therefore, in order for the nanoclusters to grow, some silicon-carbon bonds must be broken. While the amount of carbon greatly outnumbers the amount of nitrogen (coming from the TOA), if kinetic effects allow for Si-C bonds to be substituted by Si-N bonds during growth, the latter will be robust to further substitutions, as Si-N bonds are expected to be stronger than Si-C bonds at the surface of a small Si NC. To address the issue of the relative bonds strength, we calculated the Potential Energy Surface (PES) of the Si-C and Si-N bonds in SiH_3CH_3 and SiH_3NH_2 as either the methyl or the amine group is pulled from the silyl group. The bonding environment of the silyl group is locally similar to the surface of the

cluster and was kept fixed in our calculations, while the hydrogen in the methyl and amine group were allowed to relax as the Si-C and Si-N bonds are stretched. Our results show that the Si-N bond is stronger than the Si-C bond (in Figure 11, the potential well is

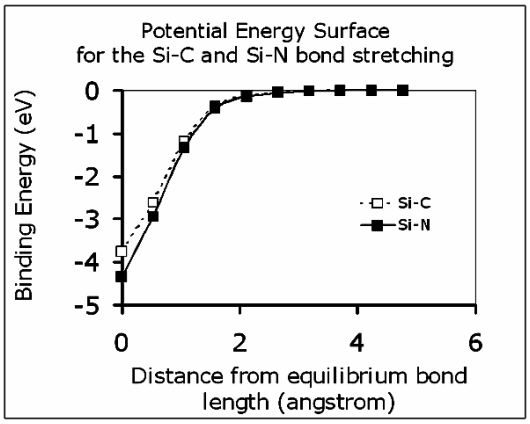

Figure 11. A comparison of the potential energy surfaces for the Si-C and Si-N bond stretching

steeper and deeper for Si-N). We estimate the binding energy to be ~ 0.6 eV larger for Si-N than for Si-C, reinforcing the hypothesis that our colloidal Si NCs have some nitrogen groups on their surfaces. This surface passivation by nitrogen could help explain the stability of the Si NCs to oxidation when they are exposed to air.

VI. Conclusion.

Silicon NCs with the sizes of 1-10 nm were synthesized in metal reactors by thermal (680^{o}C) and Au-induced (600^{o}C) decomposition of tetramethylsilane and tetraethylsilane dissolved in trioctylamine. Additional experiments conducted in glassware in the range of lower temperatures of 400-450^{o}C showed that the most likely mechanism of Si NCs formation relates to the metal-induced crystallization of amorphous Si known for

crystallization of thin amorphous Si films. HRTEM analysis of the final samples showed that NC growth proceeds by solid-phase epitaxial attachment of Si atoms to the crystal lattice of gold without evident formation of intermediate Au/Si alloys. Computational first-principles modeling made for the structural stability of Si nanocrystals with different surface groups indicate that both C- and N- containing functional groups are strongly bound to the surface of colloidal Si nanocrystals. The calculated stronger binding energy of N-containing groups correlates with the experimental observation that introducing N-containing solvents into the synthesis process increases the stability of Si NCs to oxidation.

This work was performed under the auspices of the U.S. Dept. of Energy at the University of California/Lawrence Livermore National Laboratory under contract no. W-7405-Eng-48.

Literature

(1) Ossicini, S.; Pavesi, L.; Priolo, F.; *Light Emitting Silicon for Microphotonics* Springer, New York, **2003**.

(2) Littau, K. A.; Szajowshki, P. J.; Muller, A. J.; Kortan, A. R.; Brus, L. E.; *J. Phys. Chem.* **1993**, *9*7, 1224-1230.

(3) Li, X.; He, Y.; Talukdar, S. S.; Swihart, M. T.; *Langmuir* **2003,** *19,* 8490-8496.

(4) Fojtik, A.; Henglein, A. *Chem. Phys. Lett.* **199**4, *22*1, 363-367.

(5) Heinrich, J. L.; Curtis, C. L.; Credo, G. M.; Kavanagh, K. L.; Sailor, M. J.; *Science* **1992**, *25*5, 66-68.

(6) Swerida-Krawiec, B; Cassagneau, T; Fendler, J.H.; *J.Phys.Chem. B* **1999**, 103, 9524-9529.

(7) Bley, R. A.; Kauzlarich, S. M.; Davis, J. E. Lee, H. W. H.; *Chem. Mater.* **1996**, 8, 1881-1888.

(8) Nayfeh, M.; Barry, N.; Therrien, J.; Akcakir, O.; Gratton, E.; Belomoin, G.; *Appl. Phys. Lett.* **200**1, *7*8, 1131-1133.

(9) Lie, L. H.; Duerdin, M.; Tuite, E. M.; Houlton, A.; Horrocks, B.R. *J. Electroanal. Chem.* **2002**, *538-539*, 183-190.

(10) Baldwin, R. K.; Pettigrew, K. A.; Garno, J. C.; Power, P. P.; Liu, G.Y.; Kauzlarich, S. M.; *J. Am. Chem. Soc.* **2002**, *124*, 1150-1151.

(11) Pettigrew, K.; Liu, Q.; Power, P. P.; Kauzlarich, S. M.; *Chem. Mater.* **2003**, *15*, 4005-4011.

(12) Wilcoxon, J.; Samara, G.; Provencio, P. *Phys. Rev.* **B 1999**, *60*, 2704-2714.

(13) Li, X. G.; He, Y. Q.; Swihart, M. T.; *Langmuir* **2004**, *20*, 4720-4727.

(14) Van Buuren, T.; Dinh, L.; Chase, L.; Siekhaus, W.; Terminello, L.; *Phys. ReV. Lett.* **1998**, *80*, 3803-3806.

(15) Heath, J. R. *Science* **1992**, *258*, 1131-1133.

(16) Holmes, J. D.; Ziegler, K. J.; Doty, R. C.; Pell, L. E.; Johnston, K.P.; Korgel, B. *J. Am. Chem. Soc.* **2001**, *123*, 3743-3748.

(17) English, D. E.; Pell, L. E.; Yu, Z.; Barbara, P. F.; Korgel, B. A.; *Nano Lett.* **2002**, 2, 681-685.

(18) Puzder, A.; Williamson, A.; Grossman, J.; Galli, G.; *J. Chem. Phys.* **2002**, *117*, 6721.

(19) Zhou, Z.; Brus, L.; Friesner, R. A.; *Nano Lett.* **2003**, 3, 163-167.

(20) Perdew, J. P.; Burke, K.; and Ernzerhof, M.; *Phys. Rev. Lett.* 1996, 77, 3865-3868.

(21) Gygi, F.; Lawrence Livermore National Laboratory.

(22) Helm, D. F. and Mack, E.; *J. Am. Chem. Soc.* **1937**, *59*, 60-62.

(23) Waring, C.E.; Trans.Faraday Soc.; 36, 1940, 1142-1153.

(24) Voronkov, M. G.; Dolgov, B. N.; Karpenko, G. B.; *Sov. J. Gen. Chem.* 1954, *24*, 273-275.

(25) Pell, L.; Schricker, A.; Miculec, F.; and Korgel, B.; *Langmuir* **2004**, 20, 6546-6548.

(26) R.S.Wagner and W.C.Ellis, *Appl. Phys. Lett.* **1964**, 4, 89-90 .

(27) Holmes, J. D; Johnston, K. P.; Doty, R. C.; Korgel B. A.; Science 287, **2000**, 1471-1473

(28) Bokhonov, B; Korchagin, M; *J. Alloys and Compounds*, 312, **2000**, 238-250.

(29) Wu, Y. and Yang, P.; *J. Am. Chem. Soc.* **2001**, *123*, 3165-3166.

(30) Hultman, L.; Robertsson, A.; Hentzell, H. T. G.; Engström, I., and Psaras P. A.; *J. Appl. Phys*. **1987,** 62, 3647-3655.

(31) Hayzelden, C.; Batstone, J. L.; *J. Appl. Phys.* **1993**, 73, 8279-8289.

(32) Spaepen, F.; Nygren, E.; Wagner, A. V.; in Crucial Issues in Semi-conductor Materials and Processing Technologies, NATO AS1 Series E: Applied Sciences, Vol. 222, edited by S. Coffa, F. Priolo, E. Rimini, and J. M. Poate (Kluwer Academic, Dordrecht, 1992), p. 483.

(33) Chen, M.; Zheng, A.; Hao, L., and Zhou, M. *J. Phys. Chem.* **2002**, *106*, 3077-3083.

(34) Dal Negro, L.; Yi, J. H.; Kimerling, L. C.; Hamel, S.; Williamson, A.; and Galli, G.; *Appl. Phys. Lett.* **2006**, 88, 183103.

(35) Allan, G., Delerue, C., and Lannoo, M., *Phys. Rev. Lett.* 1997, 78, 3161-3164.

(36) Rinnert. H., Vergnat, M., and Burneau, A., *J. App. Phys.* 2001, 89, 237-243.

(37) Franzo, G.; Boninelli, S.; Pacifici, D.; Priolo, F.; Iacona, F.; and Bongiorno, C.; *Appl. Phys. Lett.* **2003**, 82, 3871-3873.

(38) Jennings, H.M.; *J. Mat. Science* **1983**, 18, 951-967.

(39) Schultz, P.A. and Nelson, J.S.; *Appl. Phys. Lett*. **2001**, 78, pp. 736-738.

(40) Goss, J.P.; Hahn, I.; Jones, R.; Briddon, P.R.; Öberg, S.; *Phys. Rev. B* **2003**, 67, 045206(1-10).

(41) Jones, R.; Öberg, S.; Rasmussen, R. B.; and Nielsen, B. B.; *Phys. Rev. Lett.* **1994,** 72, 1882-1885.

(42) Lee, S.-H. and Kang, M.-H.; *Phys. Rev. B* **1998**, 58, 4903-4908.

(43) Bengio, S.; Ascolani, H.; Franco, N.; Avila, J.; Asensio, M. C.; Bradshaw, A. M.; and Woodruff, D. P.; *Phys. Rev. B* **2004**, 69, 125340 (1-9).